Dynamic heterogeneity as a strategy of stem cell self-renewal

Philip Greulich [*] [†], **Benjamin D. Simons** [*] [†] [‡]

[*]Cavendish Laboratory, University of Cambridge, JJ Thompson Avenue, Cambridge CB3 0HE, United Kingdom,[†]Wellcome Trust/CRUK Gurdon Institute, Tennis Court Road, Cambridge CB2 1QN, United Kingdom, and [‡]Wellcome Trust/MRC Stem Cell Institute, Cambridge CB2 1QR, United Kingdom

Submitted to Proceedings of the National Academy of Sciences of the United States of America

To maintain cycling adult tissue in homeostasis, the balance between proliferation and differentiation of stem cells needs to be precisely regulated. To investigate how stem cells achieve perfect self-renewal, emphasis has been placed on models in which stem cells progress sequentially through a one-way proliferative hierarchy. However, investigations of tissue regeneration have revealed a surprising degree of flexibility, with cells normally committed to differentiation able to recover stem cell competence following injury. Here, we investigate whether the reversible transfer of cells between states poised for proliferation or differentiation may provide a viable mechanism for a heterogeneous stem cell population to maintain homeostasis even under normal physiological conditions. By explaining the clonal dynamics, we show that such models of "dynamic heterogeneity" may be equally capable of describing the results of recent lineage tracing assays involving epithelial tissues. Moreover, together with competition for limited niche access, such models may provide a mechanism to render tissue homeostasis robust. In particular, in two-dimensional epithelial layers, we show that the mechanism of dynamic heterogeneity avoids some pathological dependencies which undermine models based on a hierarchical stem/progenitor organisation.

stem cell fate | stem cell heterogeneity | tissue homeostasis | stochastic models

Introduction

Stem cells are defined by their capacity to self-renew long-term while giving rise to more differentiated cell types. To achieve homeostasis, the choice between proliferation and differentiation – stem cell fate – needs to be perfectly balanced. Two generic mechanisms have been proposed to maintain a tissue cell population in homeostasis: (i) *Invariant asymmetric cell division*: after a stem cell divides, one daughter cell always remains in the stem cell compartment while the other commits to a differentiation pathway; and (ii) *Population asymmetry*: the individual fate of stem cell daughter cells may be chosen stochastically, but in balanced proportions, so that on average one daughter cell remains in the stem cell compartment and one differentiates [1, 2, 3, 4]. In recent years, experimental techniques for tracing cell lineages *in-vivo* have allowed quantitative information to be gathered on the proliferative potential of stem cells, on which hypotheses on self-renewal strategies can be tested. In particular, inducible genetic labeling methods have allowed the fate behavior of individual cells and their progeny – *clones* – to be traced over time [5, 6, 7]. Using these approaches, quantitative analyses have shown that the cell lineage data in many mammalian tissues does not conform to a pattern of invariant asymmetric division. Instead, the data is consistent with models of population asymmetric self-renewal, in which stem cell fate is chosen stochastically [8, 9, 10, 11].

In defining the quantitative fate behavior of stem cells and their differentiating progeny, most studies begin with a model in which stem and progenitor cells are organized in a one-way proliferative hierarchy. In this paradigm, under normal physiological conditions, the loss of stem cell competence and entry into a differentiation pathway is an irreversible process. However, in recent years it has been shown that, under conditions of stress or injury, cells normally committed to differentiation may reacquire stem cell competence and contribute to the long-term maintenance of tissue [12, 13, 14, 15, 16, 17, 18]. Moreover, intravital imaging studies of mouse testis and intestine suggest that, even under normal physiological conditions, adult stem cells are not homogeneous, but may transfer reversibly between states primed for proliferation and differentiation [19, 20, 21]. Finally, evidence for such stem cell flexibility has also been observed in the context of cell competition, induced through the activation of oncogenic mutation, with potential implications for the initiation of lesions and cancer [11, 22].

Taken together, these observations suggest that transition through a differentiation pathway may not involve the sequential one-way progression through a hierarchy of functionally equivalent states, but may instead be dynamic and heterogeneous, allowing cells to move reversibly between states primed for duplication or differentiation [23, 24, 25]. The genetic basis of such behavior, which we term *dynamic heterogeneity*, has been considered in a variety of contexts [21, 26, 27].

In this study, we address theoretically the question of whether tissue maintenance can be sustained by a process of dynamic stem cell heterogeneity, whether it can be discriminated from hierarchical self-renewal strategies by cell lineage tracing assays, and whether such a mechanism offers advantages in promoting robustness. Specifically, we consider a paradigm in which a (stem) cell may switch stochastically between internal "states" that may differ in their potential to enter into a differentiation pathway or to proliferate. As well as investigating the clonal fate behavior of the model system,

Significance

In many tissues, such as intestine and skin, cells are constantly turned over throughout life. To replenish cells that are lost, new cells are generated by stem cells, which divide and differentiate to maintain tissue in steady-state. The mechanisms that allow stem cells to achieve perfect self-renewal promise fundamental insights into processes leading to diseased states. Efforts to define strategies of stem cell self-renewal have placed emphasis on models in which stem cells progress one-way through a differentiation hierarchy. Here, we show that a different paradigm, in which stem cells transfer reversibly between states primed for renewal or poised for differentiation, offers a viable and robust mechanism of tissue self-renewal.

Reserved for Publication Footnotes

we also explore how the spatial distribution of cell types is affected by dynamic heterogeneity.

Results

Dynamic heterogeneity as a model of tissue maintenance. As a starting point, we consider a model of a cycling adult tissue which comprises a heterogeneous population of self-renewing progenitor cells that give rise to more differentiated progeny. However, the fate potential of individual progenitors is not invariant, but conforms to a process of dynamic heterogeneity in which, in the course of turnover, progenitors transit reversibly between states primed for proliferation or biased towards differentiation and loss. Whether these states represent defined cell types marked by signature expression of molecular markers, or whether they are simply primed by location within a niche environment, we do not distinguish. Both scenarios will lead to the same long-term clonal dynamics, the focus of the present study. Further, for simplicity, we consider only two progenitor cell states, termed A and B-type. State B is *primed* but not yet committed to terminal differentiation and loss, while the A-type cell remains in cycle. However, this bias is temporary, and cells can switch reversibly and stochastically between the two states, i.e. without division, an A-type cell can transit into a B-type cell, while a primed B-type cell can also return to the proliferative state A.

For simplicity, and to illustrate the paradigmatic features of the model, we consider a scheme in which only A-type cells have the capacity to enter into cycle while B-type cells are non-proliferative. From a biological perspective, the B-type cell may represent some transition state, poised in G_0, and deciding stochastically between re-entry into cell cycle or commitment to terminal differentiation. Furthermore, for convenience, we assume that cell division leads to asymmetric fate outcome, $A \to A+B$, noting that other "channels" of division - cell duplication or terminal division - can be captured by the model through a combination of division and "reversion" $B \longleftrightarrow A$.

Within this framework, the model dynamics is specified by the "zero-dimensional" non-equilibrium process:

$$A \xrightarrow{\lambda} A + B, \qquad A \underset{\omega_A}{\overset{\omega_B}{\rightleftarrows}} B, \qquad B \xrightarrow{\gamma} \emptyset \qquad [\mathbf{1}]$$

where λ denotes the cell division rate, and $\omega_{B,A}$ represent the transition rates from $A \to B$, respectively $B \to A$, as shown. The last process denotes the rate, γ, at which B-type cells commit to terminal differentiation and permanent loss from the A/B compartment. In the following we refer to this dynamics as the *Dynamic Heterogeneity* (*DH*) model. Finally, for simplicity, we suppose that all processes - the timing of cell division, reversion and loss through differentiation are stochastic and Markovian, with the defined average rates. Although periodicity in the timing of cell division and differentiation would impact on the short-term dynamics, the long term behaviour would be unaffected.

In the following, we will compare the kinetics of the DH model with that of a more orthodox hierarchical scheme (termed the *H model*) in which progenitor cell fate is assigned irreversibly following cell division, with only A-type cells retaining stem-like renewal potential (cf. Refs. [8, 11]),

$$A \xrightarrow{\lambda} \begin{cases} A + A & \text{Pr. } r + \Delta/2 \\ A + B & \text{Pr. } 1 - 2r \\ B + B & \text{Pr. } r - \Delta/2 \end{cases}, \qquad B \xrightarrow{\gamma} \emptyset \qquad [\mathbf{2}]$$

Here $0 \le r \le 1/2$ determines the relative frequency of symmetric vs. asymmetric cell division, and Δ parameterizes the potential bias in cell fate towards cell proliferation or differentiation. In one incarnation of the H model, the parameters r and Δ are set intrinsically and are unchanging over time [8, 11]. In other variants of the model, these parameters are variable, moderated by extrinsic cues such as the proximity to a localized niche or neighboring cell density [9, 10, 28]. Moreover, one can conceive of further adaptations of the model in which the B-type cell population has a limited renewal potential (viz. transit-amplification), or represents just one cell type in a longer hierarchy [29]. Crucially, however, the H model, as defined by Eq. **2**, is paradigmatic of all models that involve a one-way proliferative hierarchy in which the differentiating progeny of A-type cells are irreversibly committed to differentiation.

In recent years, lineage tracing studies of stratified epithelial tissues (including interfollicular epidermis, oesophagus and trachea), based on hereditary labelling using transgenic mouse models, have found that the dynamics of epithelial cell populations are consistent with models of stochastic fate choice based on the hierarchical scheme of the H model [8, 9, 11]. In the following, by comparing and contrasting the long-term behavior of these two model systems, we will investigate whether dynamic heterogeneity can provide a basis for long-term tissue maintenance, and whether its dynamics can be discriminated from that of a hierarchical cell fate scheme through clone size statistics alone.

Robustness of homeostasis. If the rates of cell division and cell fate ratios of the H and DH model are fixed, for a given arbitrary choice of parameters, the average size of the cell population is not stationary and the system is not homeostatic. Instead, the average number of A- and B-type cells would expand or contract over time. To achieve homeostasis in the H model, the net rate of progenitor cell duplication must perfectly balance differentiation and loss, requiring that the degree of imbalance, Δ, must be tuned to zero. For $\Delta > 0$, the average size of the progenitor cell compartment will grow exponentially, while for $\Delta < 0$, the progenitor population will contract until all cells are lost to differentiation. In Ref. [30] it was suggested that the dynamics of the H model can be rendered stable by imposing a feedback mechanism in which the imbalance parameter, Δ, depends on the total size of the A-cell pool. Indeed, it is known that the cell division rate can be correlated with local cell density [31] (*contact inhibition*) as well as the cell loss rate [32, 33], a phenomenon which we call *crowding feedback* (for a discussion of potential feedback mechanisms, see Refs. [34, 35, 36, 37, 38]). For the H model, such crowding feedback in the cell division rate or loss rate is not sufficient to confer stability of homeostasis. Without spatial regulation, only by controlling the cell fate bias Δ may stability be conferred (see SI).

In the DH model, the time evolution of the average densities of cell type A, n_A, and of cell type B, n_B – where $n_{B,A}$ are cell numbers normalized by volume – is given by

$$\begin{aligned} \partial_t n_A &= \omega_A\, n_B - \omega_B\, n_A \\ \partial_t n_B &= (\lambda + \omega_B)\, n_A - (\gamma + \omega_A)\, n_B \end{aligned} \qquad [\mathbf{3}]$$

Therefore, to achieve homeostasis, viz. $\partial_t n_{A,B} = 0$, the corresponding rates must also be fine-tuned such that

$$\frac{\gamma}{\lambda} = \frac{\omega_A}{\omega_B} \quad . \qquad [\mathbf{4}]$$

Under these conditions, with constant rates (i.e. no feedback), the average density of A- and B-type cells remains constant with $n_B = (\lambda/\gamma)\, n_A$. When seeded away from these values,

n_A and n_B will converge back to their steady-state values, as depicted in the flow diagram (Fig. 1A). If, however, the balance condition is not met, the populations of A- and B-type cells either decay to zero ($n_{A,B} = 0$) or grow indefinitely (cf. Fig. 1B).

Even when the systems are fine-tuned to conditions of homeostasis, without further regulation, both models are unstable towards fluctuations. In particular, in a closed system in which the size of the cell population is only finite, statistical fluctuations due to stochastic dynamics will inevitably lead to the chance extinction of the population.

The mechanism of crowding feedback can be incorporated in the models by imposing a dependence of the parameters on the average total density of cells $n = n_A + n_B$. To illustrate this, we consider the case where the cell division rate depends on n, viz. $\lambda = \lambda(n)$, and decreases monotonically with n, $\partial_n \lambda < 0$, as would be the case for contact inhibition [31]. With this implementation, the nonlinear kinetic Eqs. **3** for the DH model[1] acquire a single stable fixed point with

$$n^* = \lambda^{-1}\left(\frac{\omega_B \gamma}{\omega_A}\right), \qquad n_A^* = \rho\, n^* \qquad [5]$$

where $\lambda^{-1}(\cdots)$ denotes the inverse of the function $\lambda(n)$ and $\rho := \omega_A/(\omega_A + \omega_B)$ is an effective parameter, equivalent to the steady-state fraction of A-type cells (see SI text). In particular, for a linear response $\lambda(n) = \lambda_0 - k\, n$, where λ_0 is the unconstrained cell division rate without crowding and $k = -\partial_n \lambda > 0$ parametrizes the strength of the feedback, the stationary point is $n^* = (\lambda_0 - \omega_B \gamma/\omega_A)/k$. Inspection of the flow diagram (Fig. 1C) shows that, for a strictly linear dependence of the division rate on cell density, the stationary point is indeed globally stable. In the SI text, we show that, in fact, the system achieves a stable homeostatic state for *any* monotonically decreasing function, $\lambda(n)$, that achieves the point $\lambda = \omega_B \gamma/\omega_A$ at some given value of n. Since there is only one stable point, the system will eventually attain this homeostatic steady state.

Importantly, referring to SI text for details, a stable homeostatic state is also attained when any of the other parameters, γ, ω_A, or ω_B, are subject to negative feedback from the total cell density n. In each case, the parameters self-adjust to attain the balance condition **4**. It therefore follows that, in the case of dynamic heterogeneity, the system is robust, meaning that the failure of one feedback pathway can be compensated by another to maintain homeostasis. By contrast, for the H model, a stable homeostatic state is *only* attained if the cell fate bias Δ is a function of cell density n (see SI text). Crowding feedback in the parameters λ, γ and r is not sufficient to confer stability, so that within the framework of the model, failure of the feedback in Δ leads immediately to the loss of homeostatic stability.

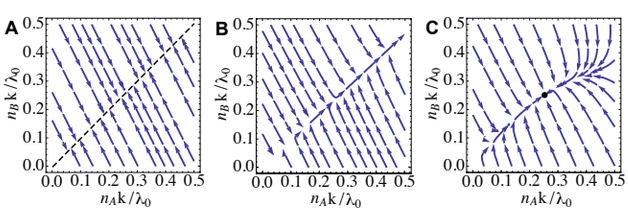

Fig. 1. Flow diagrams of the time evolution of the system, Eq. **3**, as a function of cell densities n_A, n_B measured in units λ_0/k, where $k = -\partial_n \lambda$ is the strength of the crowding feedback. We have chosen $\gamma, \omega_B = 0.5\,\lambda_0$. The arrows show the direction of the system's time evolution $(\partial_t n_A, \partial_t n_B)$. **(A)** Without crowding feedback, $\lambda = \lambda_0$, but balanced parameters $\omega_A = \lambda\,\omega_B/\gamma$. There is a line of fixed points $n_B = (\lambda/\gamma)\, n_A$, but along this line, cell densities perform neutral drift. **(B)** Without crowding feedback, $\lambda = \lambda_0$, no fate balance, $\omega_A = 2.1\,\omega_B > \lambda\,\omega_B/\gamma$. The cell population diverges. **(C)** For crowding feedback with $\lambda(n) = \lambda_0 - k\, n$ a stable fixed point emerges (black dot).

Clonal dynamics. So far we have discussed the average behavior of the DH model and its stability, but we have not addressed the dynamics of *clones*, i.e. the progeny of individually labeled cells within the steady state population. Since the dynamics of the model is stochastic, the time-evolution and survival of individual clones is variable and unpredictable. However, the dynamics of the statistical ensemble of clones can be determined. In the following we will consider the time-evolution of the *clone size distribution (CSD)* in the balanced case (fulfilling Eq. **4**), defined as the probability $P_{N_A,N_B}(t)$ to find a clone with N_A A-cells and N_B B-cells at time t when starting with a single labelled cell at $t = 0$ (*clonal induction*).

Assuming a representative labelling of cell types, starting with a single cell means that we have initially a cell of type A with probability $\rho = \omega_A/(\omega_A + \omega_B)$ and of type B with probability $(1-\rho)$, i.e. $P_{N_A,N_B}(t=0) = \rho\,\delta_{N_A,1}\,\delta_{N_B,0} + (1-\rho)\,\delta_{N_A,0}\,\delta_{N_B,1}$. For the H model, Eq. **2**, it was shown that, over time, the distribution of total clone sizes N converges onto the form [8, 28] (valid for $N \gg 1$)

$$P_N^H(t) = \frac{1}{(\Omega t)^2}\,\exp\left(-\frac{N}{\Omega t}\right), \qquad [6]$$

where $\Omega = \lambda\, r/\rho$ is the only effective parameter. The latter parameter also defines the growth rate of the average size of surviving clones, i.e. clones that retain at least one cell, $\langle N\rangle_s = (1 - P_0^H(t))^{-1} \sum_{N>0} N\, P_N^H(t) = \Omega\, t$, where $P_0^H(t) = \frac{\Omega t}{1+\Omega t}$ is the extinction probability [39]. In turn, the survival probability (norm of P_N^H in Eq. **6**) diminishes as $1/(\Omega\, t)$ at large times, so that the total cell number remains on average constant, consistent with homeostasis.

Formally, the dynamics of the clone size distribution for the DH model can be obtained from the Master equation for the probability $P^{DH}_{N_A,N_B}(t)$,

$$\begin{aligned}\partial_t P^{DH}_{N_A,N_B} &= \lambda\,[N_A\, P^{DH}_{N_A,N_B-1} - N_A\, P^{DH}_{N_A,N_B}]\\ &+ \omega_B\,[(N_A+1)\, P^{DH}_{N_A+1,N_B-1} - N_A\, P^{DH}_{N_A,N_B}]\\ &+ \omega_A\,[(N_B+1)\, P^{DH}_{N_A-1,N_B+1} - N_B\, P^{DH}_{N_A,N_B}]\\ &+ \gamma\,[(N_B+1)\, P^{DH}_{N_A,N_B+1} - N_B\, P^{DH}_{N_A,N_B}] \qquad [7]\end{aligned}$$

with the parameters subject to the balance condition, Eq. **4**. In general, a full analytic solution to the Master equation is unavailable. However, to address the long-time dependence of the probability distribution, we can proceed by implementing a van Kampen system size expansion [40] to transform the Master equation into the Fokker-Planck equation (FPE) involving a continuous function $P(N_A, N_B)$ that interpolates $P^{DH}_{N_A,N_B}$ (see SI text). The latter can be further simplified by trading the variables N_A and N_B for a slow variable $Z := N_A + [\omega_B/(\lambda + \omega_B)]\, N_B$ and a fast variable $W := N_B - [\omega_B/\omega_A]\, N_A$. With the ansatz that $P(N_A, N_B) = P(Z)\exp(-W^2/2Z)$, integration over W obtains the FPE for the distribution $P(Z)$,

$$\partial_t P(Z) = \partial_Z^2\left[(\bar{\Omega}\, Z + \Lambda) P(Z)\right] \qquad [8]$$

where the constants $\bar{\Omega}$ and Λ depend on the model parameters, as given in the SI. From the solution to this equation,

[1] Note that Eqs. **3** with crowding feedback give an exact description of the average cell density, based on the process, Eq. **1**, given that λ depends only on the *average* cell density n. If λ depends on the actual cell density, considering also fluctuations around the average, Eqs. **3** are not exact, yet they would give an accurate (mean field) approximation.

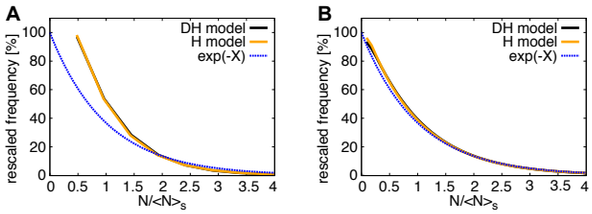

Fig. 2. Rescaled clone size distribution, showing normalized clonal frequencies as a function of rescaled clone size $X = N/\langle N\rangle_s$, where $\langle N\rangle_s = \Omega\, t$ is the average size of surviving clones (i.e. conditioned on $N > 0$). Here we choose $\omega_{A,B} = \gamma = \lambda$ in the DH model, so that $\Omega = (4/9)\,\lambda$ and we choose $r = 2/9$ for the H model to mimic this. Black lines are numerical results from the DH model (Eq. **1**) orange lines are numerical results from the H model (Eq. **2**) and dashed blue lines are the analytical result for long times, $\exp(-X)$. **(A)** At short times post-induction, $\Omega t = 1.0$, the clone statistics of the DH and H model are largely indistinguishable, but are distinct from the long-time exponential asymptotic dependence.**(B)**: At long times, $\Omega t = 10.0$, both models coincide with each other and the predicted long-term exponential dependence.

$P(Z) = (\bar{\Omega}t)^{-2}\exp(-(Z+\Lambda/\bar{\Omega})/\bar{\Omega}t)$, we obtain the full joint distribution function $P(Z,W)$. In particular, for large times $\bar{\Omega}t \gg 1$, the term $\Lambda/\bar{\Omega}$ can be neglected, and the distribution collapses onto an exponential scaling form with $\langle Z\rangle_s \sim \bar{\Omega}t$. With the Gaussian ansatz for the W-dependence, fluctuations scale as $W/Z \sim O[(\bar{\Omega}t)^{-1/2}]$, and can be neglected at large times. Taking this approximation and resubstituting $N_{A,B}$ allows to express the late-time clone size distribution as a function of $N = N_A + N_B$ only (see SI text),

$$P(N,t) = \frac{1}{(\Omega t)^2}\,\exp\left(-\frac{N}{\Omega t}\right), \qquad [9]$$

with

$$\Omega = \frac{\omega_B}{\rho}\,\frac{1+\frac{\omega_B}{\lambda}}{(1+\frac{\omega_B}{\lambda\rho})^2}\quad . \qquad [10]$$

Here we again used the parameter for the steady state A-type cell fraction $\rho = \omega_A/(\omega_A+\omega_B)$ (or alternatively $\rho = \gamma/(\gamma+\lambda)$ depending on which variable is eliminated through the balance condition). From these results it follows that the long-term clone size distribution of the DH model is identical to that of the hierarchical model. It also follows that for a slow rate of cell type conversion, $\omega_{A,B} \ll \lambda$, the clonal growth rate $\Omega \approx \omega_B/\rho$, is proportional to the switching rate, while for fast conversion, $\omega_{A,B} \gg \lambda$, we have $\Omega \approx \lambda\rho$, proportional to the cell division rate. In the latter case, each cell loses memory about its priming quickly and the two cell types behave just like a single proliferating cell population with both cell division rate and terminal differentiation rate $\lambda\rho$. This means that, between two divisions, the probability of each cell to differentiate is 1/2 which corresponds exactly to the cell fate model suggested by Marques-Pereira and Leblond in their study of esophageal maintenance [41].

To assess how rapidly the system converges onto the limiting size dependences defined above, the full solution of the Master equation can be determined at arbitrary times from numerical integration (see methods section). In Fig. 2, the numerical solutions for the distribution of clone sizes for the DH and H model are shown as a function of the clone size, scaled by the average clone size. This comparison shows that H and DH models are not distinguishable, both at short times ($t = 1/\Omega$) and at longer times ($t = 10/\Omega$). Moreover, at $t = 10/\Omega$, the distributions have already converged onto the predicted long-term scaling form, Eq. **9**. Note that for parameters other than $\omega_A = \omega_B$ slight differences between the models emerge at $t = 1/\Omega$ (see SI text). In the SI text it is also confirmed that Eq. **10** for Ω agrees well with the numerical solution of the Master equation.

Thus, when expressed in terms of the dimensionless rescaled variable $X = N/\langle N\rangle_s$, the clone size distribution of the DH model converges rapidly onto the same rescaled clone size distribution as that obtained for the H model. Therefore, based only on static clonal data alone, the dynamics of the two models cannot be discriminated.

Spatial regulation. Although both the H model and DH model can be rendered stable in the zero-dimensional system through feedback mechanisms, the advantage of the latter theory, in terms of homeostatic control, becomes apparent when the system is embedded into a defined stem cell niche geometry (see [42, 43] for niche-based regulation mechanisms). To illustrate this point, in the following we consider two concrete examples: (i) one-dimensional layers of progenitor cells, where the lowest layer is stem-like (A-cells) and higher layers are less proliferative and prone to terminal differentiation (B-cells); (ii) a two-dimensional epithelial sheet, as originally conceived for the H model in its application to basal interfollicular epidermis [44].

One-dimensional layers: As a starting point, we consider a quasi one-dimensional organization of cells in which a chain of B-type cells are maintained by an adjacent population of A-type cells, as illustrated in Fig. 3A. In the course of turnover, following the rules of the DH model (Eq. **1**) we suppose that A-type cells divide asymmetrically so that the daughter B-type cell replaces another B-type cell in the upper layer, which is presumed to be lost. Alternatively, an A-type cell (respectively B-type cell) can "switch" into a B-type cell (respectively A-type cell). However, to maintain the architecture of the tissue, this change of identity is accompanied by exchange of cell position so that the newly created A-type cell transfers to the A-type layer, and the B-type cell moves to the B-type layer.

Such dynamics mimics the process of niche-based regulation in which stem cell competence relies only on the proximity of progenitors to a localized niche environment. A similar dynamics has been conjectured to define the maintenance of the intestinal epithelium, where stem cell competence is linked to the proximity of cells to Paneth cells, which are restricted to the crypt base [19].

Effectively, the model can be reorganized as a single one-dimensional chain of alternating cell types, with each cell initially belonging to a different clone:

$$A_i\, B_j\, A_k\, B_l\, A_m \cdots \qquad [11]$$

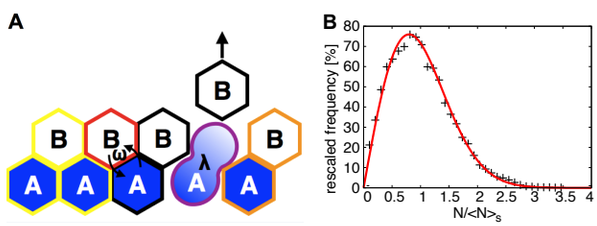

Fig. 3. Results of the DH model with spatial regulation in one dimension. **(A)** Illustration of the model dynamics, as defined by Eqs. **12** and **13**. Cells in the lowest layer are stem cell-like (A-cells) and divide asymmetrically. Cells in the upper layer (B-cells) are prone to differentiation but can also switch back into an A-type cell. The different colors of the cell boundaries represent the affiliation to different clones. **(B)** Clone size distribution as a function of $X = N/\langle N\rangle_s$, resulting from stochastic simulations. Parameters: $\omega = 0.1\,\lambda$, runtime=$100/\lambda$, system size = 10000 lattice sites. Points are simulation results and the curve is the function $P(X) = (\pi/2)\,X\exp(-\pi X^2/4)$ which is the theoretical prediction for the hierarchical cell fate model in one dimension, Eqs. **12** and **13**, and is consistent with experimental data [10].

where the indices denote the clone affiliation. The model dynamics then read:

$$A_i\,B_j \quad \xrightarrow{\lambda} \quad A_i\,B_i \qquad [12]$$

$$A_i\,B_j \quad \xleftrightarrow{\omega} \quad A_j\,B_i \qquad [13]$$

Eq. **12** represents asymmetric division wherein a neighboring B-type cell of clone j is replaced by one of clone i; and Eq. **13** represents a reversion of cell type followed by an exchange of position, with rate $\omega = \omega_A = \omega_B$, according to the DH model. (Note that such exchanges can occur in both directions.) With these rules, the configuration of A- and B-type cells remains by definition unchanged ensuring stability and homeostasis. Only the clonal composition changes over time.

To explore the clonal dynamics implied by this model, we made use of a Monte-Carlo simulation (see methods). The resulting clone size distribution is shown in Fig. 3B together with the theoretical prediction for the analogous one-dimensional hierarchical model, i.e. a one-dimensional voter model in which stem cell loss through differentiation is compensated by the replacement of a neighbor through duplication, see Ref. [28]. At long-times, both models converge onto the same distribution. Thus we conclude that the process of dynamic heterogeneity can provide a viable means to ensure long-term homeostasis and cannot be discriminated from a hierarchical model by static clonal fate data alone.

Two-dimensional cell sheet: In the following we now turn to address the implementation of cell fate models in a two-dimensional geometry, like the arrangement of cells in an epithelial basal layer. More precisely, we consider a two-dimensional lattice of cells illustrated in Fig. 4, in which all sites play host to either an A- or B-type cell. Keeping the total number of cells on the lattice fixed (viz. uniform cell density), cell division of an A-type cell only occurs when a neighboring B-type cell commits to terminal differentiation and leaves the cell sheet, e.g. migrates to upper layers of a stratified epithelium (*stratification*). The latter's site is then immediately replaced by the offspring of a neighboring dividing cell. Effectively, the constraint of fixed cell number implements (local) crowding feedback, since cell division becomes licensed only when another cell leaves the cell layer, or vice versa. For the hierarchical scheme this dynamics is captured by the following process,

$$AB \xrightarrow{\lambda} \begin{cases} AA & \text{Pr. } r + \Delta/2 \\ BA & \text{Pr. } (1-2r)/2 \\ AB & \text{Pr. } (1-2r)/2 \\ BB & \text{Pr. } r - \Delta/2 \end{cases} \qquad [14]$$

where only neighboring lattice sites are depicted (*lattice H model*). Formally, as the differentiating cell B leaves the cell layer, the neighboring proliferative A-type cell may divide to replenish the vacated site, with each progeny occupying either of the two sites with equal probability. However, this process is licensed to occur only on the condition that there is an A-type progenitor bordering the differentiated B type cell. In cases where A cells border A cells, or B cells border B cells, the system is "blocked" from cell division or stratification.

The process defined by Eq. **14** has been studied comprehensively for the balanced case $\Delta = 0$ in Ref. [44], where it was applied to the maintenance of interfollicular epidermis. There it was shown that, under these rules, the system coarsens over time and becomes increasingly inhomogeneous: the basal layer phase separates into A and B-cell rich domains that grow over time (see also Fig. 5, top rows). This process of coarsening is accompanied by the gradual cessation of tissue turnover as

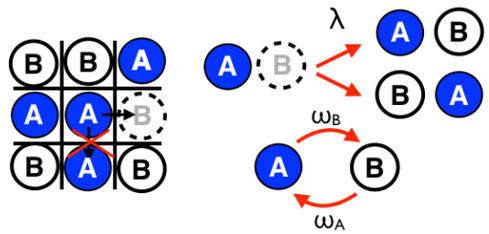

Fig. 4. Illustration of the dynamic heterogeneity model dynamics on a lattice (lattice DH model), defined by the rules of Eq. **15**. When an A-cell (blue) divides, with rate λ, a neighboring B-cell (white) commits to terminal differentiation and is lost (dashed boundary) and replaced by the offspring of the A-cell. At any time an A-type cell can turn into a B-type cell, and vice versa, according to the rules of the DH model.

only cells on the boundary of clusters can divide. Thus the system remains in a non-homeostatic state until the lattice consists of A-cells or B-cells only (fixation). Therefore, to achieve steady-state turnover, further steps must be taken to regulate proliferative activity and/or fate behavior to ensure tissue maintenance in the hierarchical model. This lack of a homeostatic state also renders the definition of a clone size distribution problematic, since it depends on the specific initial condition of the configuration of cell types.

By contrast, in the paradigm of dynamic heterogeneity, steady-state behavior of the two-dimensional system is ensured when the dynamics are implemented through the fol-

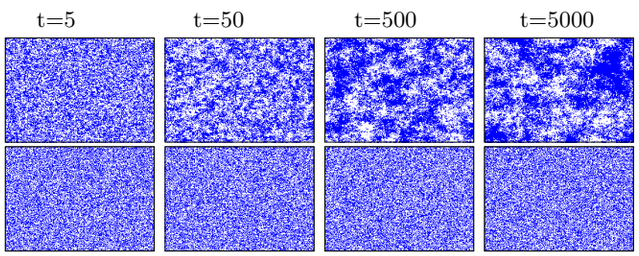

Fig. 5. Spatial distribution of cell states in the two-dimensional lattice models, at different times $\lambda t = 5, 50, 500$, and 5000, obtained by Monte Carlo simulations of the lattice H model, Eq. **14** and lattice DH model, Eq. **15**. Each pixel represents a cell in the lattice, blue pixel are A-cells, white pixels are B-cells. **Top row:** H model, r=0.1, $\Delta = 0$ **Bottom row:** DH model, $\omega_{A,B} = 0.1\,\lambda$.

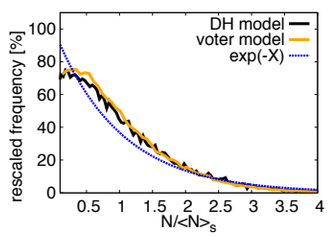

Fig. 6. Rescaled clone size distributions for two-dimensional lattice model, as a function of $X = N/\langle N\rangle_s$, where N is clone size and $\langle N\rangle_s$ the average size of surviving clones. The black line are Monte Carlo simulation results from the lattice DH model (Eq. **15**), orange are results from the voter model [46]. In the simulations we used as initial condition a randomly mixed distribution of cells, with a fraction ρ of A-type cells, and each cell representing an initial clone. The blue dashed line is an exponential distribution which is known to be the long term clone size distribution of the voter model. Parameters: lattice length $L = 1000$, $\omega_{A,B} = \lambda$, simulation time $t = 20/\Omega$, with Ω according to Eq. **10**.

lowing process (Fig. 4),

$$AB \xrightarrow{\lambda} \begin{cases} AB & \text{Pr. } 1/2 \\ BA & \text{Pr. } 1/2 \end{cases} \quad , \qquad A \underset{\omega_A}{\overset{\omega_B}{\rightleftarrows}} B \qquad [15]$$

(*lattice DH model*). Formally, although the chance development of A- or B-cell rich clusters would, respectively, inhibit cell division and differentiation, the formation and stability of these clusters is restricted by reversion events between A and B-type cells.

To illustrate the process by which the system evolves spatially, we implemented the model by Monte Carlo simulation (see Methods) to determine the lattice configurations and clonal distributions. Fig. 5 shows the time course of spatial configurations of cell types. As can be seen, for the lattice DH model (bottom row), the system remains homeostatic and homogeneous on large length scales. The reversible transition of A and B-type cells will always serve to release the deadlock, allowing the system to achieve long-term steady state behavior in which cells continuously differentiate and divide. In contrast, the lattice H model (Fig. 5, upper row) shows a persistent, non-homeostatic coarsening over the time course.

Superficially, the "pathological" coarsening behavior of the lattice H model emerged through the rigid constraint on *local* cell density, which appeared in the model through the tight-correlation of cell division with differentiation of a neighboring cell. This constraint may be relaxed by accommodating a degree of compressibility in the model. Formally, this can be achieved by accommodating vacancies or holes allowing for stratification of B-type cells uncompensated by the division of neighboring A-type cells. At the same time, A-type cells may only divide when bordering such a site vacancy. However, even under these conditions (considered in Ref. [44]), the dynamics of the lattice H model are qualitatively the same and phase separated domains of cell types emerge and grow. For the lattice DH model with site vacancies, instead, the homeostatic behavior prevails, as is shown in the SI text.

Further insight into the steady-state properties of the system can be obtained by mapping these lattice models onto a corresponding "kinetic spin model", as encountered in statistical physics. By interpreting an A-type cell as a spin $\uparrow$ degree of freedom and a B-type cell as spin $\downarrow$, the lattice DH model translates to a kinetic Ising model at infinite temperature, featuring a combination of Glauber dynamics (random spin flips) and Kawasaki dynamics (spin exchange) [45] (see SI text). Starting from any initial condition, the system flows to a homogeneous equilibrium distribution of spins, with the ratio of $\uparrow$, $\rho = \omega_A/(\omega_B + \omega_A)$ (the ratio of $\downarrow$ is $1 - \rho$), corresponding to a homeostatic state. By contrast, the lattice H model translates to a *voter model*, in which cells are stochastically and irreversible replaced by neighboring cells, following the transitions $\uparrow\downarrow \to \uparrow\uparrow$ or $\uparrow\downarrow \to \downarrow\downarrow$, respectively, with equal probability [46]. The latter model is non-ergodic, exhibiting coarsening and phase separation into large irregular domains of cell states that grow over time [46, 44]. This dynamics does not support a homeostatic state.

Tracing the clonal dynamics in the lattice DH model, we also compared the clone size distribution with results of a voter model, shown in Fig. 6 as the result of Monte Carlo simulations (see Methods). According to Fig. 6 the rescaled clone size distributions of the lattice DH-model can not be distinguished from the voter model. Since it has been rigorously shown that the voter model clone size distribution converges onto an exponential distribution, we expect this also to be the case for the two-dimensional lattice DH-model [46].

Discussion

Our study shows that dynamic heterogeneity in stem cell populations of cells reversibly switching between states that differ in their proliferative potential and their propensity towards differentiation, yields a viable mechanism to maintain homeostatic tissues. Moreover, considering the long-term clone size dependencies, a model based on dynamic heterogeneity can not be discriminated from a hierarchical model. Since hierarchical schemes involving intrinsic or extrinsic (niche-based) regulation have been used to infer self-renewal strategies in epithelial tissues such as mouse epidermis, esophagus, germ line, and intestine [8, 10, 9, 11], it follows that both dynamic heterogeneity and hierarchical fate may be equally capable of describing the results of recent lineage tracing assays. It will be important to find further short-term characteristics that can help to discriminate these models. This remains true when the model is embedded in specific spatial niche architectures that resemble tissues. Nonetheless, both dynamic heterogeneity and hierarchical balanced fate belong to the class of *population asymmetry*, in which stem cells are lost and replaced, with equal probability.

Through sensing of the cellular environment, cells may respond to variations in cell density and adjust cell division (contact inhibition) [31] and loss rate [32]. We show that with this crowding feedback a dynamically heterogeneous system adjusts to attain a stable homeostatic state. The biological background of crowding feedback, by which the cells can measure local cell density, may find a biological basis in the mechanisms of mechanosensing [47], the limited exposure to diffusible molecules released by the niche environment [20], or biochemical communication between cells [43]. Importantly, for dynamic heterogeneity, homeostasis is robust towards disruption of some crowding feedback pathways. In contrast, for hierarchical models, involving intrinsic or cell-autonomous regulation of fate, it is essential that cell fate outcomes are specified at cell division, while the control of cell division or loss rates are *not* sufficient to maintain homeostasis. Failure of this single control mechanism leads to immediate destabilization of the tissue cell population.

In a two-dimensional epithelium, however, the spatial dynamics of cell types show fundamental differences between dynamic heterogeneity and hierarchical cell fate, if left unchecked. The dynamics of the hierarchical model lead to a non-homeostatic coarsening of the tissue structure, in that regions enriched with one cell type emerge so that the cell types phase separate over time. In contrast for dynamic heterogeneity, reversible switching between states homogenizes the tissue structure, leading quickly to a macroscopically homogeneous, homeostatic cell population. The constraint of fixed total cell number in the lattice is sufficient to confer cell fate balance to the cell population in the case of dynamic heterogeneity, whereas for the hierarchical model, the ratios of symmetric cell divisions need to be fine tuned to assure balanced cell fate dynamics.

To summarize, dynamic heterogeneity provides an alternative paradigm for cell fate dynamics in homeostatic tissues, in accordance with cell lineage data. It provides a simple mechanism to balance tissue homeostasis and to homogenize the distribution of cell types in epithelial sheets. The two cell types in our model may be considered as a caricature of a single progenitor cell population carrying some memory over cell generations that renders cells primed towards proliferation or differentation. In the case of fast cell type conversion, this priming would be lost. In this limit the system can be considered as a single cell type following the random differentiation dynamics of the model introduced by Marques-Pereira

and Leblond [41]. To determine whether cell fate behaviour in epithelial tissues may involve dynamic heterogeneity, further detailed studies will be required that track cell lineages and distinguish cell states over time.

Materials and Methods

Numerical solution of Master equation. The Master equation 7 is solved by numerical integration of the constituent ordinary differential equations, when a cut-off in N_A and N_B is applied. Specifically, we considered only terms with $N_{A,B} \leq 50$, and used an adaptive Runge-Kutta method via Mathematica to solve the resulting 50×50 ordinary differential equations to obtain P_{N_A,N_B}. We then determined the rescaled clone size distribution $P(X = N/\langle N\rangle_s)$, where $\langle N\rangle_s$ denotes the average size of surviving clones ($N > 0$).

Monte-Carlo simulations of lattice models. Time is subdivided in discrete time steps $\Delta t = 1/\phi_{\max}$, where $\phi_{\max}$ is the largest transition rate out of any system configuration. At each time step Δt, a lattice site and one of its neighbors are N times randomly chosen (N= number of lattice sites). Then a random variable is generated and any possible transition, as defined by the models **12**,**14**, and **15**, with given rate ϕ, is chosen to be updated with probability $\phi\Delta t$, according to the Gillespie algorithm [48].

1. F. M. Watt and L. M. Hogan. Out of Eden: Stem Cells and Their Niches. Science, 287:1427, 2000.
2. C. S. Potten and M. Loeffler. Stem cells: attributes, cycles, spirals, pitfalls and uncertainties. Lessons for and from the crypt. Development, 110:1001, 1990.
3. M. Loeffler and B. Grossmann. A stochastic branching model with formation of subunits applied to the growth of intestinal crypts. J. Theor. Biol., 150:175, 1991.
4. B. D. Simons and H. Clevers. Strategies for homeostatic stem cell self-renewal in adult tissues. Cell, 145:851, 2011.
5. B. Sauer. Inducible gene targeting in mice using the Cre/lox system. Methods (San Diego, Calif.), 14:381, 1998.
6. P. Soriano. Generalized lacZ expression with the ROSA26 Cre reporter strain. Nature genetics, 21:70, 1999.
7. K. Kretzschmar and F. M. Watt. Lineage tracing. Cell, 148:33, 2012.
8. E. Clayton, D. P. Doupé, A. M. Klein, D. J. Winton, B. D. Simons, and P. H. Jones. A single type of progenitor cell maintains normal epidermis. Nature, 446:185, 2007.
9. C. Lopez-Garcia, A. M. Klein, B. D. Simons, and D. J. Winton. Intestinal Stem Cell Replacement Follows a Pattern of Neutral Drift. Science, 330:822, 2010.
10. A. M. Klein, T. Nakagawa, R. Ichikawa, S. Yoshida, and B. D. Simons. Mouse germ line stem cells undergo rapid and stochastic turnover. Cell stem cell, 7:214, 2010.
11. D. P. Doupé, M. P. Alcolea, A. Roshan, G. Zhang, A. M. Klein, B. D. Simons, and P. H. Jones. A single progenitor population switches behavior to maintain and repair esophageal epithelium. Science, 337:1091, 2012.
12. T. Kai and A. Spradling. Differentiating germ cells can revert into functional stem cells in Drosophila melanogaster ovaries. Nature, 428:564, 2004.
13. P. R. Tata, H. Mou, A. Pardo-Saganta, R. Zhao, M. Prabhu, B. M. Law, V. Vinarsky, J. L. Cho, S. Breton, A. Sahay, B. D. Medoff, and J. Rajagopal. Dedifferentiation of committed epithelial cells into stem cells in vivo. Nature, 503:218, 2013.
14. A. Roshan, K. Murai, J. Fowler, B. D. Simons, V. Nikolaidou-Neokosmidou, and P. H. Jones. Human keratinocytes have two interconvertible modes of proliferation. Nature Cell Biology, 18:145, 2015.
15. C. Blanpain and E. Fuchs. Plasticity of epithelial stem cells in tissue regeneration. Science, 344:1243, 2014.
16. P. W. Tetteh, H. F. Farin, and H. Clevers. Plasticity within stem cell hierarchies in mammalian epithelia. Trends in Cell Biology, 25:100, 2015.
17. H. Clevers. What is an adult stem cell? 350:4, 2015.
18. P. W. Tetteh, O. Basak, H. F. Farin, K. Wiebrands, K. Kretzschmar, H. Begthel, M. van den Born, J. Korving, F. de Sauvage, J. H. van Es, A. van Oudenaarden, and H. Clevers. Replacement of Lost Lgr5-Positive Stem Cells through Plasticity of Their Enterocyte-Lineage Daughters. Cell Stem Cell, 18:203, 2016.
19. L. Ritsma, S. I. J. Ellenbroek, A. Zomer, H. J. Snippert, F. J. de Sauvage, B. D. Simons, H. Clevers, and J. van Rheenen. Intestinal crypt homeostasis revealed at single-stem-cell level by in vivo live imaging. Nature, 507:362, 2014.
20. K. Hara, T. Nakagawa, H. Enomoto, M. Suzuki, M. Yamamoto, B. D. Simons, and S. Yoshida. Mouse spermatogenic stem cells continually interconvert between equipotent singly isolated and syncytial states. Cell Stem Cell, 14:658, 2014.
21. T. Krieger and B. D. Simons. Dynamic stem cell heterogeneity. Development, 142:1396, 2015.
22. G. Donati and F. M. Watt. Stem Cell Heterogeneity and Plasticity in Epithelia. Cell Stem Cell, 16:465, 2015.
23. M. Loeffler and I. Roeder. Tissue stem cells: definition, plasticity, heterogeneity, self-organization and models–a conceptual approach. Cells, tissues, organs, 171:8, 2002.
24. I. Roeder and M. Loeffler. A novel dynamic model of hematopoietic stem cell organization based on the concept of within-tissue plasticity. Experimental Hematology, 30:853, 2002.
25. A. D. Lander. The 'stem cell' concept: is it holding us back? Journal of Biology, 8:70, 2009.
26. S. Huang, G. Eichler, Y. Bar-Yam, and D. E. Ingber. Cell fates as high-dimensional attractor states of a complex gene regulatory network. Phys. Rev. Lett., 94:128701, 2005.
27. S. Huang. Reprogramming cell fates: Reconciling rarity with robustness. BioEssays, 31:546, 2009.
28. A. M. Klein and B. D. Simons. Universal patterns of stem cell fate in cycling adult tissues. Development, 138:3103, 2011.
29. C. J. Eaves. Hematopoietic stem cells: concepts, definitions, and the new reality. Blood, 125:2605, 2015.
30. P. Warren. Cells, cancer, and rare events: Homeostatic metastability in stochastic nonlinear dynamical models of skin cell proliferation. Physical Review E, 80:030903, 2009.
31. A. Puliafito, L. Hufnagel, P. Neveu, S. Streichan, A. Sigal, D. K. Fygenson, and B. I. Shraiman. Collective and single cell behavior in epithelial contact inhibition. Proc. Natl. Acad. Sci., 109:739, 2012.
32. G. T. Eisenhoffer and J. Rosenblatt. Bringing balance by force: live cell extrusion controls epithelial cell numbers. Trends in cell biology, 23:185, 2013.
33. E. Marinari, A. Mehonic, S. Curran, J. Gale, T. Duke, and B. Baum. Live-cell delamination counterbalances epithelial growth to limit tissue overcrowding. Nature, 484:542, 2012.
34. B. I. Shraiman. Mechanical feedback as a possible regulator of tissue growth. Proc. Natl. Acad. Sci., 102:3318, 2005.
35. A. D. Lander, K. K. Gokoffski, F. Y M Wan, Q. Nie, and A. L. Calof. Cell lineages and the logic of proliferative control. PLoS Biology, 7, 2009.
36. Z. Sun and N. L. Komarova. Stochastic modeling of stem-cell dynamics with control. Mathematical Biosciences, 240:231, 2012.
37. M. D. Johnston, C. M. Edwards, W. F. Bodmer, P. K. Maini, and S. J. Chapman. Mathematical modeling of cell population dynamics in the colonic crypt and in colorectal cancer. Proc. Natl. Acad. Sci., 104:4008, 2007.
38. H. Yamaguchi, K. Kawaguchi, and T. Sagawa. Self-Organized Criticality and Dynamical Crossover in A Stochastic Model of Cell Fate Decision. arXiv:1604.03305, 2016.
39. T. Antal and P. L. Krapivsky. Exact solution of a two-type branching process: clone size distribution in cell division kinetics. Journal of Statistical Mechanics: Theory and Experiment, 2010:P07028, 2010.
40. N. G. van Kampen. Stochastic Processes in Physics and Chemistry. North-Holland Personal Library, 2003.
41. J. P. Marques-Pereira and C. P. Leblond. Mitosis and differentiation in the stratified squamous epithelium of the rat esophagus. American Journal of Anatomy, 117:73, 1965.
42. K. B. Blagoev. Organ aging and susceptibility to cancer may be related to the geometry of the stem cell niche. Proceedings of the National Academy of Sciences, 108:19216, 2011.
43. T. Xin, V. Greco, and P. Myung. Review Hardwiring Stem Cell Communication through Tissue Structure. Cell, 164:1212, 2016.
44. A. M. Klein, D. P. Doupé, P. H. Jones, and B. D. Simons. Mechanism of murine epidermal maintenance: Cell division and the voter model. Phys. Rev. E, 77:031907, 2008.
45. A. De Masi, P. A. Ferrari, and J. L. Lebowitz. Reaction-diffusion equations for interacting particle systems. Journal of Statistical Physics, 44:589, 1986.
46. M. Bramson and D. Griffeath. Asymptotics for interacting particle systems on $\mathbb{Z}^d$. Zeitschrift fuer Wahrscheinlichkeitstheorie und Verwandte Gebiete, 53:183, 1980.
47. A. W. Orr, B. P. Helmke, B. R. Blackman, and M. A. Schwartz. Mechanisms of mechanotransduction. Developmental cell, 10:11, 2006.
48. D. T. Gillespie. Exact Stochastic Simulation of Coupled Chemical Reactions. J. Phys. Chem., 81:2340, 1977.
49. S. H. Strogatz. Nonlinear Dynamics and Chaos. Perseus Books, 1994.
50. V. Belitzky, P. A. Ferrari, M. V. Menshikov, and S. Y. Popov. A mixture of the exclusion process and the voter model. Bernoulli, 7:119, 2001.

ACKNOWLEDGMENTS. We thank Steffen Rulands for insightful discussions. This work was supported by a Research Fellowship of the German Research Foundation (DFG) and the EPSRC Critical Mass Grant.

Supplementary Information: Dynamic heterogeneity as a strategy of stem cell self-renewal

May 11, 2016

In this supplementary note we outline in detail the stability analysis of the discussed cell fate models, the analytical derivation of the clone size distribution, and support our findings for the two-dimensional lattice models.

In the simple model for dynamical heterogeneity, without spatial regulation (*DH model*), A-type cells divide asymmetrically, with rate λ, to produce one A-type and one B-type cell as daughters. A- and B-type cells can interconvert between each other with rates $\omega_{A,B}$ respectively, and B-type cells may terminally differentiate and leave the niche, with rate γ. These rules, also given as Eq. **1** in the main text, read as

$$A \xrightarrow{\lambda} A + B, \qquad A \underset{\omega_A}{\overset{\omega_B}{\rightleftarrows}} B, \qquad B \xrightarrow{\gamma} \emptyset \tag{1}$$

where cell division, loss and fate choice are assumed to occur stochastically with constant rates given above the arrows. The model thus represents a Markov process with the given stochastic transition rates. Formally, this dynamics is described by the *Master equation*, the time evolution for the probability of having N_A A-cells and N_B B-cells at time t, $P_{N_A,N_B}(t)$,

$$\begin{aligned} \partial_t P_{N_A,N_B} = {} & \lambda \left[N_A \, P_{N_A,N_B-1} - N_A \, P_{N_A,N_B} \right] \\ & + \omega_B \left[(N_A+1) \, P_{N_A+1,N_B-1} - N_A \, P_{N_A,N_B} \right] \\ & + \omega_A \left[(N_B+1) \, P_{N_A-1,N_B+1} - N_B \, P_{N_A,N_B} \right] \\ & + \gamma \left[(N_B+1) \, P_{N_A,N_B+1} - N_B \, P_{N_A,N_B} \right] \quad . \end{aligned} \tag{2}$$

To keep a compact notation we do not explicitly write the time dependence of the probabilities P_{N_A,N_B} here. This equation forms the basis for determining the time evolution of average cell densities and of the clone size distribution, i.e. the statistical distribution of the progeny of single cells.

1 Stability of the cell population

Assuming a fixed unit volume, cell densities are proportional to cell numbers, and we define the average cell densities by $n_{A,B} = \sum_{N_A,N_B=0} N_{A,B} P_{N_A,N_B}$ (note that $N_{A,B}$ stands here and in the following for "N_A and N_B, respectively". The same is valid for $n_{A,B}$). Furthermore, we assume that cell numbers are large so that the probability of extinction can be neglected, $P_{0,N_B} = P_{N_A,0} = 0$. With that, we get by using Master equation, Eq. 2, the time evolution of n_A,

$$\begin{aligned}
\partial_t n_A &= \sum_{N_A,N_B=0}^{\infty} N_A \partial_t P_{N_A,N_B} \qquad (3)\\
&= \lambda \Big[\sum_{N'_A,N'_B=0}^{\infty} N'^2_A \, P_{N'_A,N'_B} - \sum_{N'_A,N'_B=0}^{\infty} N'^2_A \, P_{N'_A,N'_B} \Big] \\
&+ \omega_B \Big[\sum_{N'_A,N'_B=0}^{\infty} (N'_A - 1) N'_A \, P_{N'_A,N'_B} - \sum_{N'_A,N'_B=0}^{\infty} N'^2_A \, P_{N'_A,N'_B} \Big] \\
&+ \omega_A \Big[\sum_{N'_A,N'_B=0}^{\infty} (N'_A + 1) N'_B \, P_{N'_A,N'_B} - \sum_{N'_A,N'_B=0}^{\infty} N'_A N'_B \, P_{N'_A,N'_B} \Big] \\
&+ \gamma \Big[\sum_{N'_A,N'_B=0}^{\infty} N'_A N'_B \, P_{N'_A,N'_B+1} - \sum_{N'_A,N'_B=0}^{\infty} N'_A N'_B \, P_{N'_A,N'_B} \Big] \ ,
\end{aligned}$$

where in each sum we redefined the indices by $N'_{A,B} = N_{A,B} \pm 1$ or $N'_{A,B} = N_{A,B}$, respectively, such that in each occurrence of P the indices are identical, giving $P_{N'_A,N'_B}$. Proceeding analogously for $\partial_t n_B$, and resubstituting the definition for $n_{A,B}$ above, we obtain the time evolution for the average cell densities (cell numbers),

$$\begin{aligned}
\partial_t n_A &= \omega_A \, n_B - \omega_B \, n_A \qquad (4)\\
\partial_t n_B &= (\lambda + \omega_B) \, n_A - (\gamma + \omega_A) \, n_B \ ,
\end{aligned}$$

which corresponds to Eq. **3**, main text. When we substitute $n_B = n - n_A$, where $n := n_A + n_B$ is the total average cell density, Eq. 5 becomes

$$\partial_t n_A(t) = f(n_A, n) \qquad \partial_t n(t) = g(n_A, n) \quad , \tag{5}$$

where we introduced the functions

$$\begin{aligned} f(n_A, n) &:= \omega_A \, (n - n_A) - \omega_B \, n_A \\ g(n_A, n) &:= \lambda \, n_A - \gamma \, (n - n_A) \quad . \end{aligned} \tag{6}$$

The steady state condition $\partial_t n_A = \partial_t n = 0$, i.e. $f(n_A, n) = g(n_A, n) = 0$, is fulfilled for

$$\frac{\lambda}{\gamma} = \frac{\omega_B}{\omega_A} \tag{7}$$

and

$$n_A^* = \rho \, n \tag{8}$$

with

$$\rho := \frac{\omega_A}{\omega_A + \omega_B} \quad . \tag{9}$$

Thus, for any n, there exists $n_A^*(n)$ that renders Eq. 5 stationary. Without any further feedback in the parameters, i.e. when all parameters are independent of cell densities n_A, n, there is not a single fixed point but a line of fixed points defined by Eq. 8. To check whether fixed points are stable, we perform a linear stability analysis. For that purpose we compute the Jacobian matrix of Eqs. 5,

$$J(n_A, n) := \begin{pmatrix} \partial_{n_A} f(n_A, n) & \partial_n f(n_A, n) \\ \partial_{n_A} g(n_A, n) & \partial_n g(n_A, n) \end{pmatrix} \quad . \tag{10}$$

A fixed point (n_A^*, n^*) is stable if both eigenvalues of J at the fixed point are negative (see Ref. [49]). This is the case if

$$\det(J(n_A^*, n^*)) > 0 \qquad \mathrm{tr}(J(n_A^*, n^*)) < 0 \quad . \tag{11}$$

For the system defined by Eqs. 5 and 6, the Jacobian reads

$$J(n_A, n) = \begin{pmatrix} -\omega_A - \omega_B & \omega_A \\ \gamma + \lambda & -\gamma \end{pmatrix} \tag{12}$$

having the trace and determinant

$$\det(J(n_A^*, n^*)) = 0 \qquad \mathrm{tr}(J(n_A^*, n^*)) = -\gamma - \omega_A - \omega_B \tag{13}$$

Since $\det(J) = 0$, the stability condition, Eq. 11, is never fulfilled. The fixed point is not stable without further assumptions on the dependence of parameters.

In the main text we discuss the situation where certain parameters depend on the total cell density (*crowding feedback*). Note that for simplicity we assumed that those parameters do only depend on the *average* cell density n, not considering fluctuations in the cell density. With this approximation, the derivation of the dynamics of average cell densities from the Master equation follows the same procedure as above (see Eq. 3), and Eqs. 5 and 6 remain valid, yet with the parameters being functions of n.

First we consider the case where only λ depends on n (*contact inhibition* [31]); below we show that the same arguments remain valid for other parameters being subject to crowding feedback. Let us assume that λ strictly decreases with n, i.e. $\lambda'(n) < 0$. As long as $\lambda^* := \gamma\,\omega_B/\omega_A$ (matching the balance condition, Eq. 7) is within the range of the function $\lambda(n)$, we get a unique fixed point $n_A^* = \rho\, n^*$ with $n^* = \lambda^{-1}(\lambda^*)$. In that case $\lambda(n^*) = \lambda^*$ and cell fate is balanced. The stability of the fixed point can again be assessed by the trace and determinant of the Jacobian matrix J, Eq. 10, of the dynamic system, Eqs. 5. Note that although we use formally the same functions f and g as in Eq. 6, the fact that $\lambda = \lambda(n)$ leads to different forms of the derivatives $\partial_n f, \partial_n g$. The trace and determinant read, evaluated at the fixed point (n_A^*, n),

$$\begin{aligned} \det(J(n_A^*, n^*)) &= -n^*\lambda'(n^*)\omega_A \\ \mathrm{tr}(J(n_A^*, n^*)) &= -\gamma - \omega_B - \omega_A + \lambda'(n^*)\rho\, n^* \end{aligned} \tag{14}$$

Since $n^* = \lambda^{-1}(\lambda^*) > 0$ and $\rho > 0$, conditions 11 are always fulfilled for $\lambda'(n) < 0$. Thus, the system is always stable for λ subject to crowding feedback with $\lambda'(n) < 0$.

Also the other model parameters may be subject to crowding feedback through a dependence on n. If $\gamma = \gamma(n)$ for example, we get

$$\begin{aligned} \det(J(n_A^*, n^*)) &= n^*\gamma'(n^*)\omega_B \\ \mathrm{tr}(J(n_A^*, n^*)) &= -\omega_A - \frac{\lambda\,\omega_A}{\omega_B} - (1-\rho)\,(n^*\gamma'(n^*) + \omega_A + \omega_B) \end{aligned} \tag{15}$$

Therefore conditions 11 are always fulfilled for $\gamma'(n) > 0$. For $\omega_B = \omega_B(n)$,

we get

$$\begin{aligned} \det(J(n_A^*, n^*)) &= n^* \gamma \, \omega_B'(n^*) \\ \mathrm{tr}(J(n_A^*, n^*)) &= -\gamma - \omega_A - \frac{\lambda \, \omega_A}{\gamma} \end{aligned} \tag{16}$$

and conditions 11 are fulfilled for $\omega_B'(n) > 0$. Finally, for $\omega_A = \omega_A(n)$, we get

$$\begin{aligned} \det(J(n_A^*, n^*)) &= -n^* \lambda \, \omega_A'(n^*) \\ \mathrm{tr}(J(n_A^*, n^*)) &= -\gamma - \omega_B - \frac{\gamma \, \omega_B}{\lambda} \end{aligned} \tag{17}$$

which again fulfills condition 11 for $\omega_A'(n) < 0$.

Thus, if any of the parameters $\lambda, \gamma, \omega_A, \omega_B$ are subject to crowding feedback, with the correct trend in the parameters' dependency on n, the stability of homeostasis is maintained.

It is important to note that the stability does not depend on the explicit form of the crowding feedback, in terms of the functions $\lambda(n), \gamma(n), \omega_{A,B}(n)$; just the correct sign of the feedback is required. Fine-tuning of parameters and of the crowding feedback mechanism is not required for stability of homeostasis. If more than one parameter exhibits crowding feedback, the homeostatic state is *robust* towards disruptions, e.g. by mutations that disrupt feedback in one of the parameters. It is sufficient if one out of four parameters retains the feedback dependence.

For the H model (Eq. **2**, main text), the dynamics are more sensitive on disruptions, even in case of crowding feedback. The time evolution of that model is given by Eqs. 5, but now with the functions

$$\begin{aligned} f(n_A, n) &= \lambda \, n_A \Delta \\ g(n_A, n) &= \lambda \, n_A - \gamma \, (n - n_A) \end{aligned} \tag{18}$$

A stationary state is only attained for

$$\Delta = 0 \tag{19}$$

giving the fixed point(s)

$$n_A^* = \rho \, n \tag{20}$$

From condition 19 it becomes immediately clear that stability of the system necessarily requires that Δ is controlled through crowding feedback. A response of λ, γ or r on the cell density n is not sufficient to keep the system in

homeostasis. To check the stability under crowding feedback of Δ, we follow the same steps as above, with $\Delta = \Delta(n)$. With this we get the Jacobian J:

$$J(n_A, n) = \begin{pmatrix} \lambda\,\Delta & \lambda\, n_A\, \Delta'(n) \\ \lambda + \gamma & -\gamma \end{pmatrix} \tag{21}$$

with determinant and trace

$$\begin{aligned} \det(J(n_A^*, n^*)) &= -n^*\,\gamma\,\lambda\,\Delta'(n) \\ \mathrm{tr}(J(n_A^*, n^*)) &= -\gamma \end{aligned} \tag{22}$$

which fulfills condition 11 for $\Delta'(n) < 0$. Thus, crowding response of Δ can in fact render the H model stable, however, this stability *only* prevails for that specific parameter responding to crowding. If regulation of this single cell fate parameter fails, crowding response of the other parameters on its own is not sufficient to maintain homeostasis.

2 Clonal evolution without spatial regulation

Here we outline how the solution of the Master equation, Eq. 2, is obtained for large $N_{A,B} \gg 1$. In that case, the probability distribution P is broad and varies only slowly between subsequent numbers $N_{A,B}$. Therefore, N_A and N_B are treated as continuous variables and P_{N_A,N_B} is approximated by a continuous function $P(N_A, N_B)$. Then, differences of the probability in neighboring values of N_A, N_B can be approximated by a second order Taylor expansion (corresponding to a *van Kampen expansion* [40]):

$$\begin{aligned} P_{N_A+\delta_A,N_B+\delta_B} &\approx P(N_A,N_B) + \partial_{N_A} P(N_A,N_B)\cdot\delta_A + \partial_{N_B} P(N_A,N_B)\cdot\delta_B \\ &+ 1/2\,\partial^2_{N_A} P(N_A,N_B)\cdot\delta_A^2 + \partial_{N_A,N_B} P(N_A,N_B)\cdot\delta_A\delta_B + 1/2\,\partial^2_{N_B} P(N_A,N_B)\cdot\delta_B^2 \end{aligned} \tag{23}$$

In the following, we only consider the balanced case for which $\omega_A/\omega_B = \gamma/\lambda$ (see Eq. 7). Substituting the Taylor approximation, Eq. 23, in Eq. 2,

gives the *Fokker-Planck equation (FPE)*

$$\begin{aligned}
\partial_t P(N_A,N_B) &= \left[K\lambda + (1+K)\omega\right] P(N_A,N_B) \\
&+ \left[\omega(N_A - N_B\,K - K + 1)\partial_{N_A} P(N_A,N_B)\right. \\
&+ \left[K\lambda + (K-1)\omega + (\lambda+\omega)(N_B K - N_A)\right]\partial_{N_B} P(N_A,N_B) \\
&+ 1/2\left[\omega\,(1+K) + \omega\,N_A + \omega K\,N_B\right]\partial^2_{N_A} P(N_A,N_B) \\
&+ 1/2\left[K\lambda + \omega(1+K) + (\lambda+\omega)(N_A + N_B\,K)\right]\partial^2_{N_B} P(N_A,N_B) \\
&- \left[\omega(1+K+N_A+N_B K)\right]\partial_{N_A,N_B} P(N_A,N_B)
\end{aligned} \tag{24}$$

Where for convenience we introduced the effective parameters $K := \omega_A/\omega_B = \gamma/\lambda$ to eliminate γ and used $\omega := \omega_B$. In the following we want to obtain analytical solutions for the FPE when the "fast" degrees of freedom are integrated out. For that purpose, we introduce auxiliary variables $Z := N_A + \frac{\omega}{\lambda+\omega} N_B$ and $W := N_B - N_A/K$. When substituting these variables, and rearranging derivatives by partial integration, the FPE reads, expressed in the new variables (Z,W),

$$\begin{aligned}
&\partial_t P(Z,W) = \partial_W\left[W(\omega + K(\lambda+\omega))\,P(Z,W)\right] \\
&+ \partial^2_W\left[\left(W\,\frac{K(\lambda-\omega)\omega - \omega^2 + K^2\omega(\lambda+\omega) + K^3(\lambda+\omega)^2}{2K\omega + 2K^2(\lambda+\omega)}\right.\right. \\
&+\; Z\,\frac{(\lambda+\omega)(\omega + 2K\omega + K^2(\lambda+\omega))}{K\omega + K^2(\lambda+\omega)} + \left.\left.\frac{\omega + 3\,K\omega + 3\,K^2\omega + K^3(\lambda+\omega)}{2\,K^2}\right)\,P(Z,W)\right] \\
&+ \partial_W\partial_Z\left[\left(W\,\frac{\lambda\omega(\omega - K(\lambda+\omega))}{(\lambda+\omega)(\omega + K(\lambda+\omega))} - Z\frac{2\lambda\omega}{\omega + K(\lambda+\omega)}\right.\right. \\
&\qquad\left.\left. -\frac{(1+2K)\lambda\omega}{K(\lambda+\omega)}\right)\,P(Z,W)\right] \\
&+ \partial^2_Z\left[\left(W\frac{K\lambda\omega(K(\lambda+\omega) - \omega)}{2(\lambda+\omega)(\omega + K(\lambda+\omega))} + \frac{\lambda\omega(\lambda + K\lambda + K\omega)}{2(\lambda+\omega)^2}\right.\right. \\
&\qquad\left.\left. +Z\,\frac{K\lambda\omega}{\omega + K(\lambda+\omega)}\right)\,P(Z,W)\right]
\end{aligned} \tag{25}$$

Now we make the Gaussian ansatz

$$P(Z,W) = P(Z)\cdot\exp(-W^2/(2\,Z))/\sqrt{2\pi Z} \tag{26}$$

and integrate out the fast variable W. For this ansatz, boundary terms of the integration vanish since $\lim_{W\to\pm\infty} W^\alpha P(Z,W) = 0$ for any α. Thus all

terms starting with the differential operator ∂_W vanish by intergration over W, and we arrive at

$$\partial_t P(Z) = \partial_Z^2 \left[(\Lambda + \bar{\Omega}\, Z) P(Z) \right] \tag{27}$$

with

$$\begin{aligned} \Lambda &= \frac{\lambda\omega(\lambda + K\lambda + K\omega)}{2(\lambda+\omega)^2} \\ \bar{\Omega} &= \frac{K\lambda\omega}{\omega + K(\lambda+\omega)} \end{aligned} \tag{28}$$

Here we have used that $\int_{-\infty}^{\infty} dW\ W\, P(Z,W) = 0$ and $\int_{-\infty}^{\infty} dW\ P(Z,W) = P(Z)$ for the Gaussian ansatz. This partial differential equation is solved by

$$P(Z,t) = \frac{1}{(\bar{\Omega}t)^2} \exp\left(-\frac{Z + \Lambda/\bar{\Omega}}{\bar{\Omega}t} \right) \quad . \tag{29}$$

After all we want to find the clone size distribution as a function of the total cell number N, $P(N)$, where $N = N_A + N_B$. From the solution, Eq. 29, it follows that $\langle Z \rangle = \bar{\Omega}t - \Lambda/\bar{\Omega}$, thus for large times $t \gg \Lambda/\bar{\Omega}^2$, the term $\Lambda/\bar{\Omega}$ can be neglected for $Z \sim \langle Z \rangle$. Since the distribution of W is Gaussian with variance Z, and $Z \sim t$, fluctuations in W are of order $O((\bar{\Omega}t)^{1/2})$, so that $N_B = N_A/K + O((\bar{\Omega}t)^{1/2})$, and we can approximate

$$\frac{Z}{\bar{\Omega}t} = \frac{N_A + \frac{\omega}{\omega+\lambda} N_B}{\bar{\Omega}t} = \frac{(\omega + K\omega + K\lambda)^2}{K(1+K)\omega\lambda(\omega+\lambda)} \frac{N}{t} + O(t^{-1/2}) \quad . \tag{30}$$

Neglecting $O(t^{-1/2})$ for large times and substituting Eq. 30 into Eq. 29, we find the clone size distribution as a function of N

$$P(N,t) = \frac{1}{(\Omega t)^2} \exp\left(-\frac{N}{\Omega t} \right), \tag{31}$$

with

$$\Omega = \frac{\lambda\, \omega\, K(1+K)(\lambda+\omega)}{(\omega + K\,\omega + K\,\lambda)^2} \tag{32}$$

Using the effective parameter $\rho = \omega_A/(\omega_B + \omega_A)$, which corresponds to the steady state fraction of A-type cells, we can substitute $K = \rho/(1-\rho)$ and $\omega = \omega_B$, and arrive at the form used in the main text:

$$\Omega = \frac{\omega_B}{\rho} \frac{1 + \frac{\omega_B}{\lambda}}{(1 + \frac{\omega_B}{\lambda\rho})^2} \tag{33}$$

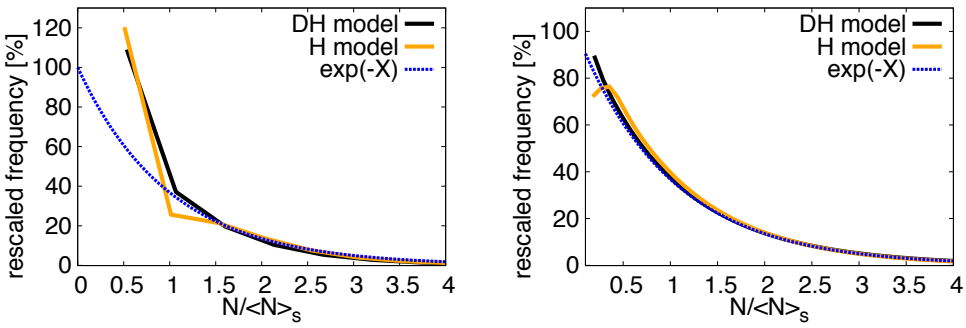

Figure 1: Rescaled clone size distribution. Clonal frequencies as a function of rescaled clone size $X = N/\langle N\rangle_s$, where $\langle N\rangle_s = (1-P_0)^{-1}\sum_{N>0} NP_N$ is the average size of surviving clones. Chosen parameters are $\gamma = \omega_A = \omega_B/3$, $\omega_B = \lambda$ in the DH model, so that $\Omega = (8/25)\,\lambda$, and we choose $r = 2/25$ for the H model to mimic this (Note that in contrast to the main text, here $\omega_B \neq \omega_A$). Black lines are numerical results from the DH model, orange lines are numerical results from the H model (see main text), and dashed blue lines are the analytical result for long times, $\exp(-X)$. **(A)** At short times post-induction, $\Omega t = 1.0$ **(B)**: At long times, $\Omega t = 10.0$.

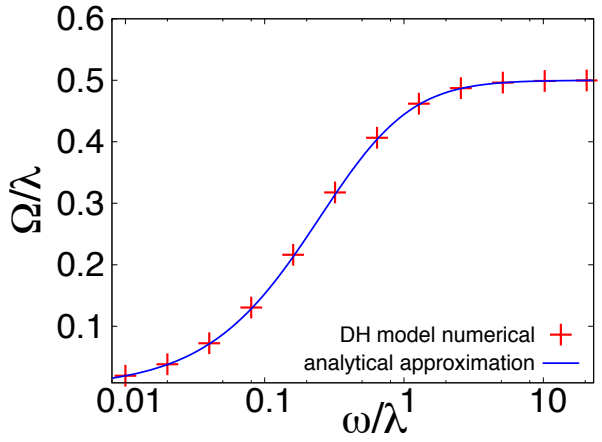

Figure 2: Theoretical prediction for the scaling parameter Ω as defined in Sec. 2, according to Eq. 32 (blue line), together with results for Ω from numerical solution of the original Master equation, Eq. 2 (points, see Methods section) for $K = 1$.

By comparing with the numerical solution of the original Master equation, Eq. 2, we show in Fig. 2, main text, that Eq. 31 approximates well the clone size distribution of the DH model. In Fig. 2, main text, we used the parameters $\omega_A = \omega_B$ which led to almost identical solutions for both the H and DH model. However, it turns out that this perfect match is due to the special case $\omega_A = \omega_B$; in the case $\omega_A \neq \omega_B$ a discrepancy between the models becomes apparent at short times, $t = 1/\Omega$, as shown in Fig. S1. At late times, $t = 10/\Omega$, nonetheless, both solutions coincide again and resemble the analytical result, Eq. 31.

In Fig. S2 it is also shown that Eq. 32 matches well the numerical results for Ω as obtained from solving the Master equation numerically.

3 Spatial regulation in lattice model

3.1 Imbalance in the hierarchical lattice model

For the DH model implemented on a lattice geometry (*lattice DH model*), no fine-tuning of the parameters is required to achieve homeostasis. In that case the constraint of fixed cell number acts in a same way as crowding feedback in the non-spatial model to confer a stable state. Here we check whether this is also the case for the lattice H model. For that purpose, we implemented the lattice H model, Eq. **15**, main text, with $\Delta \neq 0$. In Fig. S3 the time course of the cell type configuration is shown for a slight cell fate bias $\Delta = 0.01$. Even for such a small imbalance A-type cells take over the whole lattice, and no homeostatic state of coexisting cell types is attained.

3.2 Coarsening

In this section we argue by general analytical considerations that for the lattice H model the system always coarsens, characterized by a diverging correlation length and the absence of a homeostatic state, in contrast to the lattice DH model which attains a homeostatic (equilibrium) state with a finite correlation length.

The lattice models as defined in the main text can be simplified as follows, when the clonal identity of cells is neglected. We denote X as a randomly chosen cell in the lattice, while Y is one of its 4 neighboring cells and $\bar{X}$ is the opposite cell type of X ($\bar{X} = B$ if $X = A$ and vice versa). In this

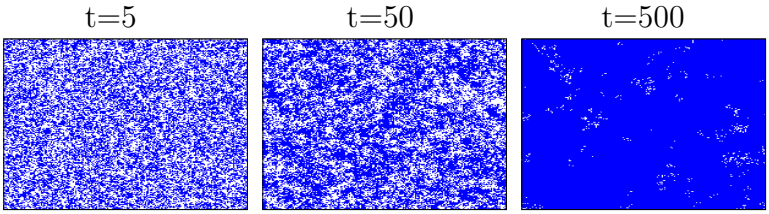

Figure 3: Spatial distribution of cell types in the lattice H model, with a symmetric division ratio $r = 0.1$ and a non-zero cell fate imbalance $\Delta = 0.01$, obtained by Monte Carlo simulations at different times t (time unit is $1/\lambda$). Each pixel represents a cell in the lattice, blue pixel are A-cells, white pixels are B-cells.

terminology the lattice H model reads

$$X + Y \to X + X \qquad \text{with rate } \lambda\, r \qquad \text{symmetric divisions} \tag{34}$$

$$X + Y \to Y + X \qquad \text{with rate } \lambda\,(1 - 2r)/4 \qquad \text{asymmetric division + swap sites} \tag{35}$$

and the DH model can be expressed as

$$X + Y \to Y + X \qquad \text{with rate } \lambda/4 \qquad \text{asymmetric division + swap sites} \tag{36}$$

$$X \leftrightarrow \bar{X} \qquad \text{with rates } \omega_B, \omega_A \qquad \text{state switching} \tag{37}$$

To clarify, the correspondence to the lattice models introduced in the main text are the following:

- Event 34 describes symmetric divisions: cell divisions may only occur at an AB pair site, viz. when the B-type cell is lost. Without loss of generality we allow that cell division may happen both when the A-cell is selected and when the B-cell of this pair is selected. This means that cell division is executed only at half the normal rate, $\lambda/2$, to compensate for the doubled probability to choose a pair of cells to update. Either of the two sites is selected with equal probability, thus redefining the rules such that symmetric renewal occurs when the A site is selected, $AB \to AA$, and symmetric differentiation occurs when the B site is selected, $BA \to BB$, is equivalent to symmetric divisions.

- Asymmetric division allows two configurations of daughter cells, $AB \to AB$ or $AB \to BA$. Events 35 and 36 correspond to the second option, while in the first case the system configuration does not change.

- Event, 37 comprises the two switch events $A \to B$ and $B \to A$, with rates ω_B and ω_A respectively.

Note that when $X = Y$, execution of processes 34, 35, 36 lead to no change of configurations, which is consistent with the lattice update rule that cell division only occurs when an A-cell is next to a B-cell. This simplification is only possible since clonal identity is not considered, otherwise the chosen update rule does explicitly depend on the values of X and Y.

The dynamics 34 - 37 are equivalent to paradigmatic models of statistical physics. To see this, let us interpret the state of a cell at a given site as a *spin* where A denotes $\uparrow$ and B denotes $\downarrow$.

- Event 34 is equivalent to the dynamics of a *voter* model [46]. This stochastic process exhibits coarsening with domain sizes growing on average over time t as $\sim t^{1/2}$ in one dimension and $\sim t/\ln(t)$ in a two-dimensional lattice.

- Events 35 and 36 correspond to the spin exchange dynamics under *Kawasaki* spin update rules of an *Ising model* at infinite temperature.

- Event 37 corresponds to the spin-flip dynamics in a *Glauber* update scheme of the Ising model at infinite temperature.

Hence, in this picture, the lattice H model corresponds to a voter model with Kawasaki spin exchange dynamics. For that model, it was shown that any domain front between $\uparrow$- and $\downarrow$-domains is stable (i.e. ergodic) if there is no bias in the spin exchange dynamics [50]. This means that domain walls evolve on large scales as in the voter model, so that domain sizes grow over time. This is also consistent with studies on the combination of voter and Kawasaki dynamics in 2 dimensions [44], that have shown that the correlation length diverges and the system performs coarsening, even for large ratios of Kawasaki dynamics. Thus for the H model on a lattice, non-homeostatic coarsening and divergence of the correlation length prevails.

The DH model corresponds to the combination of Glauber (spin-flip) and Kawasaki (spin-exchange) dynamics at infinite temperature. This is an

implementation of a kinetic Ising model and leads to the stationary (equilibrium) state the Ising model at infinite temperature, characterized by a finite correlation length and a density of up-spins $\rho = \omega_A/(\omega_A + \omega_B)$. Thus, no coarsening emerges and a homeostatic state is reached for the lattice DH model.

3.3 Mobile vacancies in the lattice

Here we want to consider the model alternative where B-type cells may be lost even if there is no adjacent dividing A-type cells. In that case the B-type cell leaves a vacancy $\emptyset$ ($B \to \emptyset$) when lost. We assume that this vacancy may move in the lattice by exchanging sites with neighbors randomly, until it is adjacent to an A-type cell which then divides to fill the vacancy. This is defined by the following rules:

$$A\emptyset \xrightarrow{\lambda} XX, \quad B\emptyset \xrightarrow{\sigma} \emptyset B, \quad B \xrightarrow{\gamma} \emptyset \tag{38}$$

where the identity of daughter cells after division, $A\emptyset \to XX$ depends on the model implementation. For the lattice H model, we have

$$XX = \begin{cases} AA \text{ Pr. } r \\ BA \text{ Pr. } (1-2r)/2 \\ AB \text{ Pr. } (1-2r)/2 \\ BB \text{ Pr. } r \end{cases}, \tag{39}$$

for the lattice DH model

$$XX = \begin{cases} BA \text{ Pr. } 1/2 \\ AB \text{ Pr. } 1/2 \end{cases}, \tag{40}$$

and furthermore the cell fates switch reversibly:

$$A \xrightarrow{\omega_B} B, \quad B \xrightarrow{\omega_A} A \tag{41}$$

Here we consider the limit $\sigma, \lambda \to \infty$, i.e. whenever a vacancy emerges it immediately explores the lattice until finding an A-type cell that divides and fills the vacancy with its progeny. With this choice of parameters, cell loss and division are still coupled, but this coupling may be between A- and B-type cells that are far from each other.

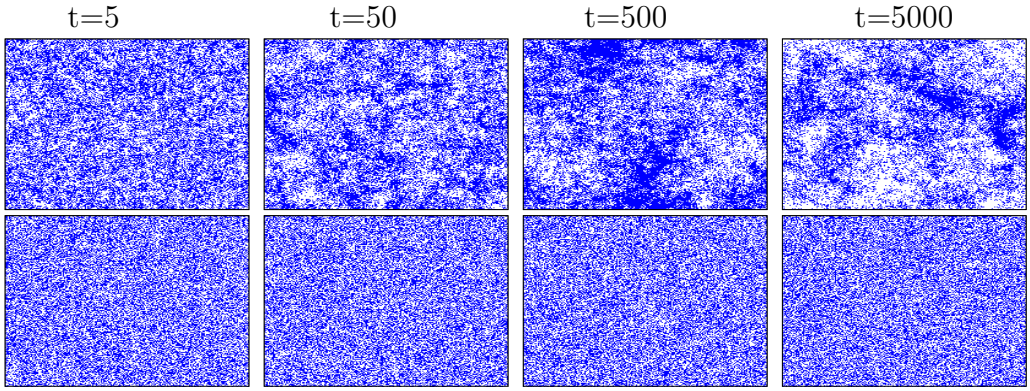

Figure 4: Spatial distribution of cell states in the two-dimensional lattice model with vacancies (Eq. 38, at different times $t = 5$, 50, 500, and 5000 in units $1/\lambda$. Results are obtained by Monte Carlo simulations for the lattice H model, Eq. 39, and for the lattice DH model, Eq. 40. Each pixel represents a cell in the lattice, blue pixel are A-cells, white pixels are B-cells. **Top row:** lattice H model, $r = 0.1$, **Bottom row:** lattice DH model, $\omega_{A,B} = 0.1\,\lambda$.

For this model we show the time course of cell configuration in Fig. S4, both for the lattice H model and the lattice DH model. We can see that the same phenomenology as without holes prevails: in the lattice H model the system coarsens without reaching a homeostatic state (as was also shown for the same model in Ref. [44]), while for the DH model, the system is well mixed and assumes quickly a homeostatic state.